Journal of Electronic Research and Application, 2026, Volume 10, Issue 5
http://ojs.bbwpublisher.com/index.php/JERA
Online ISSN: 2208-3510
Print ISSN: 2208-3502

Analysis of Metro Car Ride Comfort Based on FBG Measurement and Validation

Zhaoqing Guan[1]*, Guanlan Li[1], Jiatian Yu [2], Wenqing Yang[3], Siqun Ma[1]

[1]Zhan Tianyou College of Dalian Jiaotong University (CRRC College), Dalian 116028, Liaoning, China
[2]Guidao Jiaotong Polytechnic Institute, Shenyang 110023, Liaoning, China
[3]Zhengzhou Depot of China Railway Zhengzhou Group Co., Ltd., Zhengzhou 450000, Henan, China

***Corresponding author*:** Zhaoqing Guan, gzqq12345@qq.com

Abstract: To accurately evaluate the ride comfort of metro cars, this paper collects and analyzes carbody vibration acceleration on an urban metro line using Fiber Bragg Grating (FBG) measurement technology. Through trend term removal and bandpass filtering preprocessing, effective vibration signals are extracted, and characteristic parameters such as the Sperling ride comfort index and dominant frequencies are calculated. Simultaneously, a SIMPACK vehicle dynamics model is established with American Level 5 track spectrum excitation. Simulation results are compared with measured data to validate model reliability, and the model is then used to provide simulation comparisons for ride comfort analysis. Results show that the vertical ride comfort indices at two measurement points are 1.939 and 1.956, and lateral indices are 2.015 and 2.045, all reaching the "Excellent" level. Relative errors of ride comfort indices between simulation and measurement range from 5.2% to 6.7%, indicating high model credibility. Frequency domain analysis shows that the vertical dominant frequency of the carbody is 1.50 Hz and the lateral dominant frequency is 1.75 Hz, with good consistency between measurement and simulation. This work provides an effective method for metro car ride comfort evaluation based on FBG measurements, and offers quantitative basis for parameter calibration of metro train dynamics models.

Keywords: Metro train; FBG measurement; Model validation; Ride comfort index; Error tracing

Online publication: Jun 29, 2026

1. Introduction

With the continuous expansion of global urban rail transit networks and rapid growth in passenger demand, the running safety, ride comfort, and passenger comfort of metro trains have become core issues in railway transportation development [1]. Train ride comfort comprehensively reflects the dynamic performance of the vehicle system, directly affecting operational safety, passenger experience, equipment service life,

and line maintenance costs [2]. Therefore, accurate measurement and evaluation of carbody vibration response is fundamental for optimizing vehicle dynamics performance and condition monitoring [3]. In vibration measurement, traditional electrical acceleration sensors face significant limitations in the strong electromagnetic interference and complex mechanical vibration environment of metro cars [4]. Their analog signals are susceptible to electromagnetic noise from traction systems, leading to reduced signal-to-noise ratio. Fiber Bragg Grating (FBG) sensing technology, with its anti-electromagnetic interference characteristics, offers distinct advantages in monitoring metro trains [5].

In engineering practice, establishing vehicle models using multi-body dynamics simulation software for dynamics analysis has become an important means to study and optimize suspension system performance. However, the accuracy of simulation models heavily depends on the precision of input parameters, and discrepancies often exist between model predictions and actual train operating conditions [6]. Therefore, using real vehicle test data to validate simulation models is a critical step to ensure their engineering guidance value [7].

Based on FBG measurement data, this paper conducts multi-dimensional validation of a metro train dynamics model. First, carbody vibration response is obtained through line tests, and ride comfort indices are extracted after signal preprocessing. Then, a SIMPACK vehicle dynamics model is established, and simulations are performed under the same operating conditions. Finally, model accuracy is validated from both time and frequency domains, and the measured and simulated ride comfort indices are compared to quantify model errors and trace main influencing factors, providing a basis for subsequent model calibration.

2. Principle of fiber Bragg grating sensing

2.1. Fiber Bragg grating sensing principle

An optical fiber is a symmetrical cylindrical dielectric structure consisting of multiple layers, generally composed of a core, cladding, and coating [8]. In practical applications, an outer sheath is added to protect the fiber. The core and cladding are the main structures for light wave propagation and are key components. The coating and sheath provide physical protection, isolate stray light, enhance fiber strength, and reduce long-distance transmission loss.

The transmission principle of light waves in optical fibers mainly relies on total internal reflection [9]. Because the refractive index of the core is greater than that of the cladding, when the incident angle exceeds the critical angle corresponding to the air refractive index, incident light does not refract but propagates entirely along the core by reflection. Thus, the fiber uses total internal reflection to confine electromagnetic waves in the core and guide them along the fiber axis.

A Fiber Bragg Grating (FBG) is a sensing element fabricated by ultraviolet laser exposure, which permanently changes the refractive index of the fiber core periodically [10]. Its sensing principle is that when light propagates through the grating, the grating reflects wavelengths satisfying the Bragg condition while transmitting most other wavelengths. The principle of fiber Bragg grating sensing is shown in Figure 1.

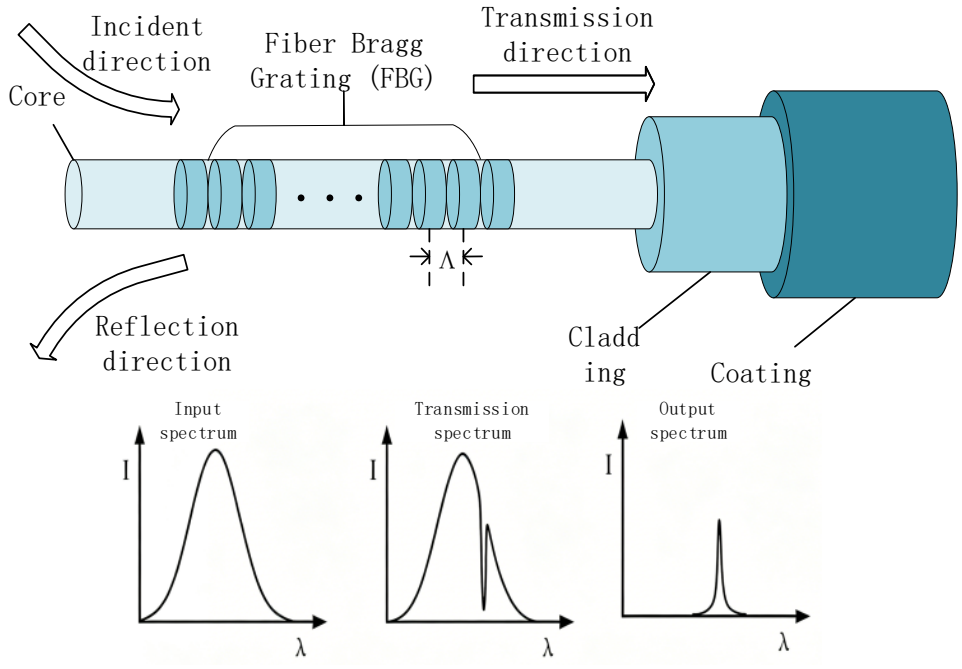

Figure 1. Schematic of FBG sensing principle.

Let the effective refractive index of the core be n_{eff} and the grating period be Λ. Then the central wavelength of reflected light is:

$$\lambda_B = 2n_e ff\Lambda \tag{1}$$

This formula demonstrates the theoretical basis of FBG as a sensing element: the central wavelength is proportional to the core refractive index and grating period. When external physical quantities change these variables, the measured variation can be inferred by capturing wavelength shifts.

2.2. FBG acceleration sensing characteristics

FBG acceleration sensors utilize the wavelength modulation principle of gratings. External vibration changes the grating pitch, which is converted into a corresponding wavelength shift, thereby measuring acceleration magnitude. The mechanical model can be simplified as a single-degree-of-freedom mass-spring system. Under acceleration, the mass experiences inertial force, causing slight changes in FBG length and thus grating period [11].

The relationship between acceleration and wavelength shift is:

$$\frac{\Delta\lambda_B}{\lambda_B} = \frac{ma}{EA} \tag{2}$$

where E is the elastic modulus of the fiber, A is the cross-sectional area of the fiber, m is the mass of the proof mass, and a is acceleration. It can be seen that wavelength shift is strictly proportional to vibration acceleration, and the sensitivity and frequency response range can be adjusted by changing the proof mass.

3. Ride comfort monitoring test

3.1. Hardware configuration of monitoring test

The ride comfort monitoring test mainly uses FBG acceleration sensors, fiber optic transmission cables, an FBG interrogator, an industrial computer, wireless transmission equipment, and an uninterruptible power supply.

3.1.1. FBG acceleration sensor

The test uses the OS7100 FBG acceleration sensor, as shown in Figure 2,which is optimized based on FBG technology, with a measurement range from DC to several hundred Hz and high accuracy and stability for low-frequency signal detection. The sensor features a metal-sealed design and armored optical cable protection, offering resistance to electromagnetic interference, lightning strikes, and corrosion, allowing direct outdoor installation.

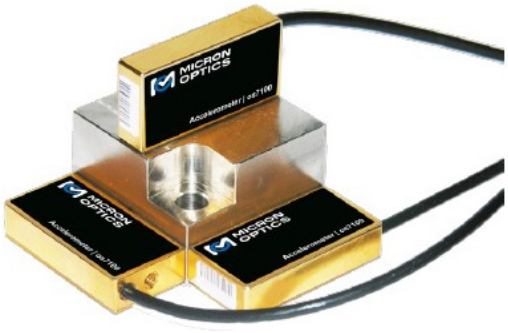

Figure 2. OS7100 FBG acceleration sensor.

Main performance parameters: operating temperature -40~80°C, sensitivity approximately 16 pm/g, frequency range DC~300 Hz, maximum response frequency approximately 700 Hz, maximum shock 100 g. Dimensions: 38×9×19 mm, weight 28 g. Center wavelength range 1512~1588 nm, peak reflectivity >70%.

3.1.2. FBG interrogator

The test uses the SM130 FBG interrogator, as shown in Figure 3,which features high power, high storage rate, and multi-channel data acquisition. The interrogator has 4 optical channels, wavelength range 1510~1590 nm, stability 2 pm typical, 5 pm maximum, each channel can connect up to 80 sensors. Maximum scan frequency 1 kHz, optical connector type FC/APC.

Figure 3. FBG interrogator.

The accompanying software system enables sampling frequency setting, wavelength-to-physical quantity conversion formula definition, file storage format selection, and storage mode configuration (continuous, periodic, or triggered).

3.2. Sensor installation positions and layout

According to GB/T 5599-2019 "Railway vehicles – Specification for dynamic performance assessment and test identification", acceleration sensors are arranged on the carbody floor at positions 1 m from the front and rear bogie centers [12]. As shown in Figure 4, sensors are installed at measurement points 1 and 2.

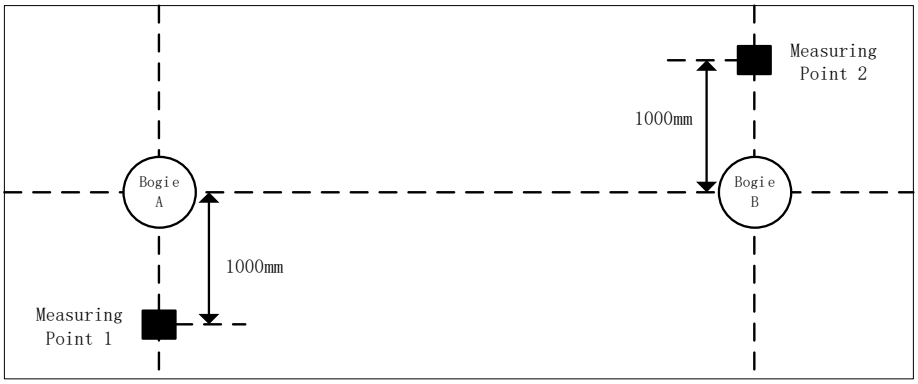

Figure 4. Sensor installation positions.

Sensors are attached using adhesive fixation, with specialized adhesive connecting the sensor to the structure. This method does not affect the structure, is simple and quick, and has wide applicability. Before installation, the mounting surface must be cleaned to ensure firm adhesion. After installation, the interrogation system is calibrated to compensate for wavelength drift caused by curing.

3.3. Ride comfort calculation

Vehicle ride comfort is evaluated using the Sperling index. According to vibration frequency classification, the vibration amplitude of each frequency band is obtained through spectrum analysis, the individual comfort index W_i for each band is calculated, and then the overall comfort index is obtained:

$$W = \sqrt[10]{\sum_{i=1}^{n} W_i^{10}} \tag{3}$$

The formula for the ride comfort index of a single frequency band is:

$$W_i = 3.57 \sqrt[10]{\frac{A_i^3}{f_i}} F\left(f_i\right) \tag{4}$$

where A_i is the vibration acceleration (m/s²), f_i is the vibration frequency (Hz), and $F(f_i)$ is the frequency correction coefficient. The correction coefficients for vertical and lateral vibrations are selected according to GB/T 5599-2019.

According to GB/T 5599-2019, the ride comfort classification is: Level 1 (Excellent) < 2.5, Level 2 (Good) 2.5–2.75, Level 3 (Acceptable) 2.75–3.0.

The overall ride comfort monitoring process is shown in Figure 5. First, FBG acceleration sensors

collect carbody vibration signals, which are converted to digital signals by the FBG interrogator. Then data preprocessing (including trend term removal and bandpass filtering) is performed. Next, spectrum analysis is conducted on the preprocessed signals to obtain vibration amplitudes in each frequency band. Sperling indices are calculated per frequency band using Equation (4). Finally, the overall Sperling index W is synthesized using Equation (3), outputting vertical and lateral ride comfort indices and corresponding grades.

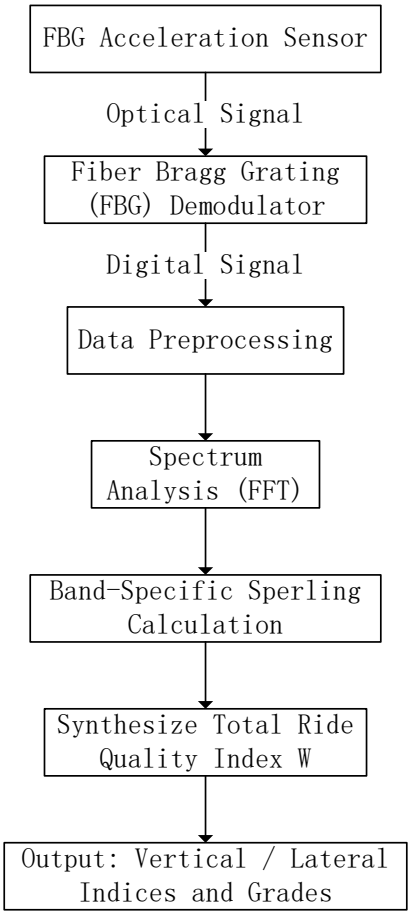

Figure 5. Ride comfort monitoring flowchart.

4. Vehicle dynamics modeling

4.1. Whole vehicle system dynamics computational model

This paper uses SIMPACK software to establish the metro train dynamics model. SIMPACK is maturely applied in railway transportation, employing recursive algorithms and parametric modeling, offering advantages such as convenient modeling and accurate calculation results.

To improve computational efficiency while maintaining simulation accuracy, the following reasonable simplifications and assumptions are made: wheelsets and bogie frames are considered rigid bodies since their elasticity is much smaller than that of the suspension system; rail elastic deformation is neglected; because traction force has little effect on vehicle dynamics, motor torque output-related excitations are ignored; the mass of the suspension system is neglected, and primary and secondary suspensions are modeled as linear massless spring-damper elements.

Based on metro train dynamics parameters, the dynamics model is built step by step: wheelset → wheel-rail contact → bogie → whole vehicle model. The Body element defines masses and moments of inertia of the carbody, bogie frame, and wheelsets. Force Elements define primary and secondary suspension devices. Joints define connection types.

Some parameters of the metro train dynamics model are listed in Table 1. The established metro car dynamics model is shown in Figure 6.

Table 1. Parameters of vehicle system dynamics model

Dynamics parameter	Value	Unit
Wheelset mass	1420	kg
Bogie frame mass	2550	kg
Carbody mass	21920	kg
Primary spring vertical stiffness	1.7	MN/m
Primary spring longitudinal stiffness	6.6	MN/m
Primary spring lateral stiffness	10.4	MN/m
Secondary spring vertical stiffness	2.75	MN/m
Secondary spring longitudinal stiffness	1.3	MN/m
Secondary spring lateral stiffness	1.3	MN/m
Primary spring vertical damping	0.05	MN·s/m
Primary spring longitudinal damping	0.05	MN·s/m
Primary spring lateral damping	0.05	MN·s/m
Secondary spring vertical damping	0.4	MN·s/m
Secondary spring longitudinal damping	0.3	MN·s/m
Secondary spring lateral damping	0.3	MN·s/m
Wheelset yaw moment of inertia	985	kg·m²
Bogie frame yaw moment of inertia	1980	kg·m²
Bogie frame roll moment of inertia	1050	kg·m²
Bogie frame pitch moment of inertia	1750	kg·m²
Carbody yaw moment of inertia	617310	kg·m²
Carbody roll moment of inertia	14890	kg·m²
Carbody pitch moment of inertia	617310	kg·m²
Vehicle wheelbase	12.6	m
Wheelset axle distance	2.2	m
Vehicle length	19	m

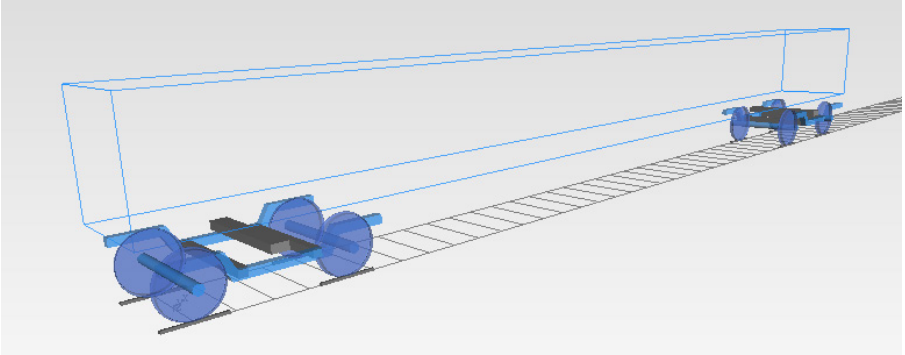

Figure 6. Metro car dynamics model.

4.2. Track irregularity model

Track irregularities are the main factor causing lateral and vertical dynamic responses of trains. Track irregularities include vertical irregularities (longitudinal level, cross level) and lateral irregularities (alignment, gauge).

In vehicle system dynamics simulation, the American Level 5 track spectrum is selected as the excitation input. The main formulas for the American Level 5 spectrum are:

Vertical irregularity (longitudinal level):

$$S_v(\Omega) = \frac{kA_V\Omega_C^2}{\Omega^2(\Omega^2+\Omega_C^2)} \tag{5}$$

Lateral irregularity (alignment):

$$S_a(\Omega) = \frac{kA_a\Omega_C^2}{\Omega^2(\Omega^2+\Omega_C^2)} \tag{6}$$

Cross level and gauge irregularities:

$$S_c(\Omega) = S_g(\Omega) = \frac{4kA_V\Omega_C^2}{(\Omega^2+\Omega_s^2)(\Omega^2+\Omega_C^2)} \tag{7}$$

Where Ω is spatial angular frequency, A_a and A_v are cutoff frequencies, Ω_c and Ω_s are roughness constants, and k is a safety factor.

5. Model validation and result analysis

5.1. Measured signal analysis

First, FBG acceleration signals collected from actual tests on an urban metro line are preprocessed. A least squares method (3rd-order polynomial) is used to remove trend terms, eliminating low-frequency drift caused by train acceleration/deceleration and line gradients. According to GB/T 5599-2019, a 4th-order Butterworth bandpass filter is applied to carbody vertical and lateral accelerations, with an analysis frequency band of 0–40 Hz. After preprocessing, effective vibration signals are extracted, and time-domain statistical features and frequency-domain characteristics are calculated.

The test operating speed is approximately 50 km/h on a straight section. Measurement data indices for points 1 and 2 are shown in **Table 2** and **Table 3**.

Table 2. Measured data indices at Point 1

Direction	RMS (m/s²)	Sperling ride comfort index	Dominant frequency (Hz)
Vertical	0.2245	1.939	1.50
Lateral	0.1528	2.015	1.75

Table 3. Measured data indices at Point 2

Direction	RMS (m/s²)	Sperling ride comfort index	Dominant frequency (Hz)
Vertical	0.3207	1.956	1.50
Lateral	0.1995	2.045	1.75

5.2. Simulation condition setup

Based on the SIMPACK metro train dynamics model, simulation conditions identical to the measurements are set: operating speed 50 km/h, straight line without gradient, integration step 1 ms, simulation duration 60 s. Track irregularity excitation uses the American Level 5 track spectrum. The simulation sampling frequency is set to 2048 Hz, consistent with the measured FBG sensor sampling frequency. Carbody vibration responses from simulation are filtered identically, and RMS, power spectral density, dominant frequency, and Sperling ride comfort indices are extracted.

5.3. Time and frequency domain comparison

Vibration data from measurement Point 1 are selected as measured data for comparison with simulation data at the corresponding position in the SIMPACK model.

5.3.1. RMS comparison

RMS reflects the average energy level of vibration signals and is a fundamental indicator for evaluating vibration intensity. Comparison of RMS between simulation and measurement is shown in **Table 4**.

Table 4. Comparison of carbody vibration acceleration RMS

Direction	Measured RMS (m/s²)	Simulated RMS (m/s²)	Absolute error (m/s²)	Relative error
Vertical	0.2245	0.242	0.0175	7.8%
Lateral	0.1528	0.165	0.0122	8.0%

From **Table 4**, simulated RMS values are slightly higher than measured ones. This trend is consistent with the subsequent deviation direction of ride comfort indices, indicating that the model's predicted vibration energy is conservative, which is acceptable for engineering safety assessment. The relative error for vertical RMS is 7.8%, and for lateral 8.0%, both within the typical 10% requirement for engineering applications, demonstrating that the model can reproduce the vibration energy level of the actual vehicle reasonably well.

5.3.2. Frequency domain comparison

The Welch method is used to estimate power spectral density (PSD) of acceleration signals, with Hanning window, 50% overlap, FFT points 4096, frequency resolution 0.1 Hz. **Figures 7 and 8** show the PSD comparisons of carbody vertical and lateral acceleration (0–40 Hz band).

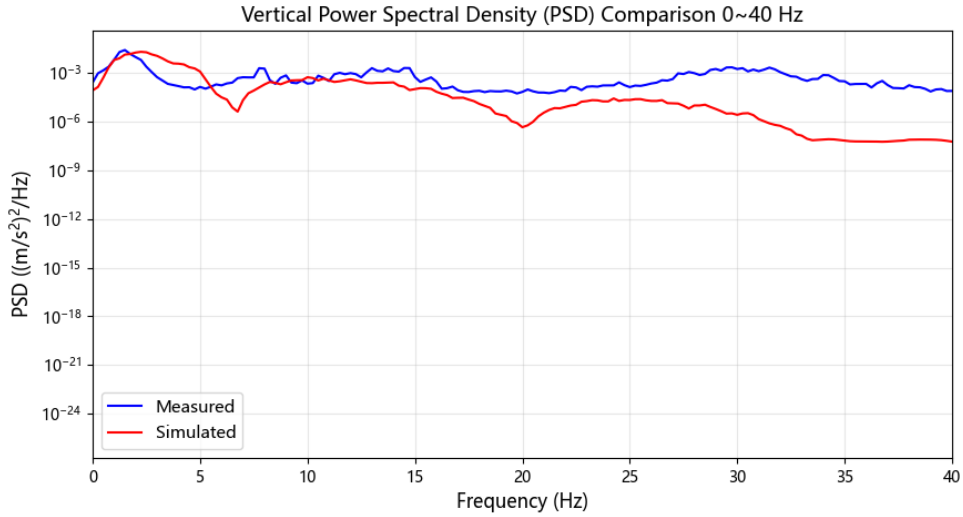

Figure 7. Vertical acceleration PSD comparison.

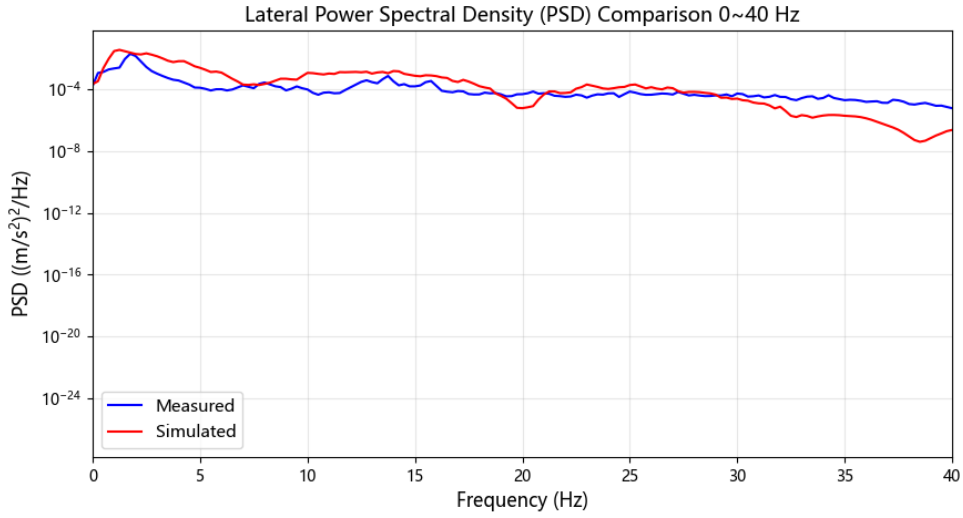

Figure 8. Lateral acceleration PSD comparison.

From the vertical PSD comparison (Figure 7), the dominant frequencies of simulation and measurement are basically consistent, both around 1.50 Hz, corresponding to the carbody heave mode. In the 2–5 Hz band, simulated PSD is slightly higher than measured; in the 5–25 Hz band, simulated PSD remains slightly higher; in the 25–40 Hz band, the difference gradually increases, with simulation values significantly higher than measurement. This trend indicates that the simulation model overpredicts vibration response in mid-to-high frequency bands, possibly related to the high-frequency energy setting of the track spectrum input or simplifications in the high-frequency dynamic characteristics of the suspension system.

From the lateral PSD comparison (Figure 8), the dominant frequencies of simulation and measurement are basically consistent, both around 1.75 Hz, corresponding to the carbody yaw mode. Over the entire 0–40 Hz band, the simulated and measured PSD curves generally agree well, but in the 30–40 Hz high-frequency

band, measured values gradually exceed simulated ones, indicating that actual lines have high-frequency local excitations (such as rail welds, switch impacts) that simulation cannot fully reproduce. Overall, the simulated and measured PSDs are within the same order of magnitude, with consistent distribution trends in main frequency bands. The model can effectively reflect the vibration energy distribution characteristics of the actual vehicle, though some deviation exists in the high-frequency band.

To further quantify the agreement of frequency domain characteristics, dominant frequencies of acceleration from simulation and measurement are extracted and compared in Table 5.

Table 5. Comparison of carbody vibration acceleration dominant frequencies

Direction	Measured dominant frequency (Hz)	Simulated dominant frequency (Hz)	Absolute error (Hz)	Relative error
Vertical	1.50	1.70	0.20	13.3%
Lateral	1.75	1.65	0.10	5.7%

From Table 5, the simulated vertical dominant frequency is slightly higher than measured, with a relative error of 13.3%; the simulated lateral dominant frequency is slightly lower than measured, with a relative error of 5.7%. The larger vertical dominant frequency error may be related to parameter values of carbody mass, suspension stiffness, or heave mode damping ratio settings in the model. The lateral dominant frequency error is small, indicating that the model predicts the yaw mode accurately. Overall, the dominant frequency deviations are within acceptable ranges, and the model can effectively reflect the main vibration modal frequencies of the actual vehicle.

5.4. Ride comfort index analysis

Sperling ride comfort indices from simulation and measurement are calculated according to GB/T 5599-2019, with measured values represented by Point 1. Results are shown in Table 6.

Table 6. Comparison of ride comfort indices

Direction	**Measured value**	**Simulated value**	**Absolute error**	**Relative error**
Vertical	1.939	2.04	0.101	5.2%
Lateral	2.015	2.15	0.135	6.7%

From **Table 6**, the measured vertical and lateral ride comfort indices are 1.939 and 2.015, respectively, both less than 2.5, reaching the “Excellent” level. The simulated vertical and lateral ride comfort indices are 2.04 and 2.15, also within the “Excellent” range. The simulated ride comfort indices are slightly higher than measured, indicating that the model’s predicted ride comfort is conservative, which is positive for engineering safety assessment. The relative error for the vertical ride comfort index is 5.2%, and for the lateral 6.7%, both within 10%, verifying that the established SIMPACK model has high engineering credibility. Additionally, both measurement and simulation show that lateral ride comfort indices are higher than vertical ones, consistent with the characteristic of relatively prominent lateral excitation on urban metro lines.

5.5. Error tracing analysis

Based on the above data comparisons, the model agrees well with measured data in three aspects: time-domain energy (RMS), frequency-domain dominant frequencies, and ride comfort indices, with most error indices controlled within 10%. This indicates that the established SIMPACK dynamics model has high simulation accuracy and engineering application value.

The main identified error sources include:

(1) Nonlinearity and time variance of suspension parameters: In practice, the damping of anti-yaw dampers and air springs varies with amplitude and frequency, whereas the simulation uses constant parameter simplifications. This may be the main cause of response deviations in mid-to-high frequency bands;

(2) Simplification of wheel-rail contact geometry: The simulation uses a new wheel profile, while the actual wheels experience wear after operation, resulting in changes in equivalent conicity that affect lateral dynamic response. This may be one reason why the lateral error is slightly larger than the vertical error;

(3) Simplification of local line characteristics: The simulation uses a stationary random track spectrum, whereas actual lines have local features such as rail welds and switches. These features have some influence on high-frequency vibrations. However, the American Level 5 spectrum, as a standard spectrum, can effectively reflect the main irregularity energy distribution of the line, and overall agreement is good.

6. Conclusion

Based on FBG line measurement data, this paper conducts multi-dimensional validation and error analysis of a metro train SIMPACK dynamics model. The main conclusions are as follows:

(1) FBG sensors performed well in actual metro train tests, accurately capturing carbody vibration response. The adopted signal preprocessing method and analysis according to GB/T 5599-2019 effectively extracted vibration characteristics. The vertical Sperling indices at two measurement points are 1.939 and 1.956, and lateral indices are 2.015 and 2.045, all reaching the “Excellent” level;

(2) The simulated and measured acceleration frequency-domain power spectra have generally consistent distribution trends in main frequency bands, with good agreement in dominant frequencies, indicating that the established vehicle dynamics model is accurate and credible for engineering applications;

(3) The relative errors of vertical and lateral Sperling ride comfort indices between simulation and measurement are 5.2% and 6.7%, respectively, and RMS relative errors are 7.8% and 8.0%, all within acceptable engineering ranges. The model can be used to assist in analyzing factors affecting ride comfort;

(4) The errors mainly originate from the nonlinear characteristics of suspension parameters and simplifications in wheel-rail contact geometry. Future work will focus on parameter calibration of the dynamics model based on measured data, with emphasis on considering the nonlinear characteristics of suspension components.

Funding

Transportation Science and Technology Plan Project of the Department of Transportation of Liaoning Province (Project No.: 202151)

Disclosure statement

The author declares no conflict of interest.

References

[1] Zhang C, Kordestani H, Shadabfar M, 2023, A combined review of vibration control strategies for high-speed trains and railway infrastructures: Challenges and solutions. Journal of Low Frequency Noise, Vibration & Active Control, 42(1): 272–291.

[2] Zhai W, 2015, Vehicle-Track Coupled Dynamics, 4th ed. Science Press, Beijing.

[3] High-speed Railway Vibration and Noise Testing Technology, China Railway Publishing House, Beijing, 2018.

[4] Xu L, Gao G, Peng C, et al., 2023, Train structural health monitoring method integrating fiber optic sensing and piezoelectric sensing. Journal of Railway Science and Engineering, 20(7): 2763–2772.

[5] Yang T, Wang G, 2023, Research on load and dynamic stress monitoring system for key structures of high-speed maglev train based on fiber Bragg grating. Rolling Stock, 61(3): 93–97+131.

[6] Xiao X, 2022, Vehicle system dynamics performance analysis based on SIMPACK. Machinery Manufacturing & Automation, 2022(5): 1–5.

[7] Carpio J, et al., 2025, Validation and Calibration of Energy Models with Real Vehicle Data from Chassis Dynamometer Experiments, arXiv, 2025: 2503.21057.

[8] Ding B, Zhao Q, Chen D, et al., 2024, Progress in fiber Bragg grating pressure sensing technology and applications. Acta Optica Sinica, 50(3): 23001801. (in Chinese)

[9] Fan S, Liu X, Yang W, 2025, Comprehensive experimental teaching design of fiber grating sensing. Optical Technique, 51(2): 145–152.

[10] Guo Y, Xiong L, Zhou X, et al., 2022, High-performance fiber Bragg grating inclination sensor for mechanical equipment. Journal of Mechanical Engineering, 58(8): 571–579.

[11] Zhu J, Jiang Y, Xue W, 2024, Method for measuring acceleration using fiber Bragg grating. Optoelectronics·Laser, 35(4): 456–462.

[12] State Administration for Market Regulation of the People's Republic of China, Standardization Administration of the People's Republic of China, 2019, GB/T 5599-2019 Railway vehicles – Specification for dynamic performance assessment and test identification, China Standard Press, Beijing.